PAPER

Casiopeinas® third generation, with indomethacin: synthesis, characterization, DFT studies, antiproliferative activity, and nanoencapsulation†

Yokari Godínez-Loyola,[a] Jesús Gracia-Mora, [ID][a] Iván D. Rojas-Montoya, [ID][a] Luis Felipe Hernández-Ayala, [ID][a] Miguel Reina,[a] Luis Antonio Ortiz-Frade,[b] Luisa Alondra Rascón-Valenzuela,[c] Ramón Enrique Robles-Zepeda,[c] Virginia Gómez-Vidales,[d] María Josefa Bernad-Bernad*[a] and Lena Ruiz-Azuara [ID]*[a]

Seven new Casiopeinas® were synthesized and properly characterized. These novel compounds have a general formula [Cu(N−N)(*Indo*)]NO₃, where *Indo* is deprotonated indomethacin and N−N is either bipyridine or phenanthroline with some methyl-substituted derivatives, belonging to the third generation of Casiopeinas®. Spectroscopic characterization suggests a square-based pyramid geometry and voltammetry experiments indicate that the redox potential is strongly dependent on the N−N ligand. All the presented compounds show high cytotoxic efficiency, and most of them exhibit higher efficacy compared to the well-known cisplatin drug and acetylacetonate analogs of the first generation. Computational calculations show that antiproliferative behavior can be directly related to the volume of the molecules. Besides, a chitosan (CS)−polyacrylamide (PNIPAAm) nanogel was synthesized and characterized to examine the encapsulation and release properties of the [Cu(4,7-dimethyl-1,10-phenanthroline)(*Indo*)]NO₃ compound. The results show good encapsulation performance in acidic conditions and a higher kinetic drug release in acidic media than at neutral pH. This result can be described by the Peppas−Sahlin model and indicates a release mechanism predominantly by Fick diffusion.

1. Introduction

In Ancient Near East civilizations, metals were already used for medicinal purposes,[1,2] but it was only at the beginning of the 20th century when Paul Elrich established the modern inorganic medicinal chemistry concept. Elrich developed the first inorganic chemotherapeutic agent, *Salvarsan*, that was implemented for syphilis treatment.[3,4] Years later, Barnett Rosenberg discovered the cytotoxic properties of cisplatin, which was introduced as a clinical anticancer drug in 1978.[5–8] In this regard, cisplatin has been the most notorious anticancer metallodrug, and its derivatives have been proved effective against lung, ovarian, esophageal, and neck cancer.[9–13] However, these compounds show severe adverse effects in patients, including hair loss, nephrotoxicity, ototoxicity, neuropathy, and myelotoxicity.[14–17] Furthermore, drug resistance is another very serious limitation of platin-based cancer chemotherapy.[18]

To overcome the drug resistance and the side effects several approaches have been developed, one of them is the drug design based on the essential trace metals such as copper. Copper is a micronutrient with a fundamental role in several biological processes such as mitochondrial metabolism[19] and cellular protection against oxidant species.[20] Although copper is essential in healthy cells, an elevated concentration favors angiogenesis, tumor growth and metastasis.[21,22] This difference in copper response between the tumoral and normal cell environments is the reason for the evolution of copper complexes as anticancer agents. These complexes show high cytotoxicity and they have proved anticancer performance. Recently, copper complexes have been synthesized with several donor atoms (N, O, S and P principally) ligand-based. Some of them as disulfiram, elesclomol, and thiosemicarbazones based ligands are currently in clinical trials.[23–25] These complexes are multitarget and multifunctional agents, and their anticancer performance involves several mechanisms. Copper chelators diminish their endogenous concentration and difficult the growth of malignant cells and angiogenesis. Other systems interact with proteosomes and inhibit their function.[26] For instance, a Cu-esclemol complex can interfere in the ferredoxin function and

[a]*Facultad de Química, Universidad Nacional Autónoma de México, Av. Universidad 3000, Circuito Exterior S/N, CU, Ciudad de México, C.P. 04510, Mexico. E-mail: bernadf@comunidad.unam.mx; lenar701@gmail.com*

[b]*Centro de Investigación y Desarrollo Tecnológico en Electroquímica, Sanfandila, Querétaro, Mexico*

[c]*Departamento de Ciencias Químico-Biológicas, Universidad de Sonora, Boulevard Luis Encinas y Rosales S/N, Hermosillo, Sonora, C.P. 83000, Mexico*

[d]*Instituto de Química, Universidad Nacional Autónoma de México, Av. Universidad 3000, Circuito Exterior S/N, CU, Ciudad de México, C.P. 04510, Mexico*

† Electronic supplementary information (ESI) available. See https://doi.org/10.1039/d2ra03346a

produce cuproptosis, a cell death that occurs independently of apoptosis pathways.[27]

In the search for new anticancer drugs with fewer side effects, Casiopeinas®, mixed chelate copper complexes, have been synthesized, reported, and patented.[28,29] Casiopeinas® are well-known copper compounds with proved potent anticancer activity; their general formulae is $[Cu(N–N)(L–L)]^{n+}$ (n = 1, 2), where N–N = 1,10-phenanthroline or 2,2′-bipyridine and L–L = secondary ligand being different bidentate chelate, one of them (CasIII-ia: $[Cu(44'dmbipy)(acac)]^+$) is now being tested in clinical trials. The second-generation possess a neutral L–L ligand as ethylenediamine and substituted benzimidazoles and 1,2-dianilines,[30,31] and the third generation is characterized by the presence of molecules with O–O donor atoms as secondary ligands with proven biological activity as curcumin and indomethacin.[32] The main difference between first and third generation of Casiopeinas® is that the secondary ligand for first generation is any monocharged N–O or O–O donor atoms molecule, and for third generation is a molecule with the same donor atoms, also monocharged, but these molecules present by themselves a proved biological activity. The insertion of this type of secondary ligand may modulate and increase the anticancer activity and the anti-inflammatory activity that would enhance the antitumor one. However, the main mechanism of action that have been obtained for the first generation would not be different for the third generation because the main weak oxidant property and ROS generation and apoptosis induction, through the reduction of Cu^{II} to Cu^{I} is supposed to be the same. The mechanisms of action have been studied in more than 20 compounds, founding the ROS generation towards induction of apoptosis, interaction with DNA, and their nuclease action.[33–35] These compounds represent a viable, attractive, and accesible alternative for cancer treatment, including lung, cervix, and breast cancer. Additionally, Casiopeinas® show low toxicity against normal cells, which suggests high selectivity.[36] It has been also demonstrated that Casiopeinas® possess a multitarget cytotoxicity mechanism that converges in the cell apoptosis induction.[37–39] In addition, in silico studies suggest that all the three Casiopeinas® generations can act as antiviral agents by the inhibition of the main protease of SARS-CoV-2.[40]

Indomethacin is a nonsteroidal anti-inflammatory drug (NSAID) that inhibits cyclooxygenases (COX).[41] In cancer disease, COX-2, an isoform of COX enzymes, is expressed in numerous solid tumors and their neovasculature.[42] Thus, the use of NSAIDs as COX-2 inhibitors emerge as a strategy to limit tumoral growth. In fact, in vitro, and in vivo models show a proliferation rate decrease, an increment in the apoptosis, and an attenuation of metastasis.[43] Copper–indomethacin complexes also have been investigated as anticancer agents in mammary cells.[44] These complexes show cytotoxic activity in micromolar order and a COX-2 inhibitors with a better performance than indomethacin.[45] From above, indomethacin complexes represent good candidates to possess relevant antiproliferative properties.

Although the investigation of therapeutic systems has been a prolific research field in the last decades, drug delivery on specific target cells to treat cancer has remained an elusive and complex topic.[46] One interesting strategy to overcome this obstacle is drug encapsulation with polymers or nanoparticles as vehicles.[47–51] Encapsulation involves the modification of different physicochemical and biochemical features including solubility, stability, and Burst release, resulting in the prevention of drug degradation, increased therapeutic efficacy and decreased side effects.[52–56] On that matter, hydrogels present an available and versatile alternative to pharmaceutical applications, especially since they do not dissolve in physiological temperature and pH.[57–59] Hydrogels are generally made of low-cost materials, possess tunable three-dimension structures, remarkable mechanic properties, high water content, and great biocompatibility.[60] Hydrogels made of chitosan, a biopolymer of acetylated/ deacetylated N-acetyl-β-D-glucosamine, have received great attention for their inherent biological properties and considerable swelling in an aqueous medium.[61,62] This is a valuable property since these systems can respond to media changes counting pH and once cross-linked to thermo-responsive polymers, temperature,[63,64] allowing their focalized use for drug release. These features are suitable for anticancer drugs since tumor microenvironments are characterized by acid pH and increased temperature.[65]

Herein, the synthesis, characterization, DFT studies, and antiproliferative activity of novel third Casiopeinas® generation are presented. These compounds have general formula $[Cu(N–N)(Indo)]NO_3$, where Indo is the deprotonated form of indomethacin and N–N are different methyl-substituted bipyridines and phenanthrolines. In addition, the synthesis and characterization of a nanopolymer formed by chitosan (CS), poly-N-isopropylacrylamide (pNIPAAm), and N,N'-methylenebis(acrylamide) (MBA) is also presented. Finally, the studies of $[Cu(4,7-dimethyl-1,10-phenanthroline)(Indo)]NO_3$ nano-encapsulation efficiency and kinetics release are discussed.

2. Materials and methods

2.1. Chemicals

All chemicals and solvents were used as received from Aldrich Chemical Co. and J.T. Baker.

2.2. Physical measurements

Thermo Scientific/Flash 2000 was employed for elemental analysis determination. FT-IR spectra were recorded on KBr disks in a Nexus Thermo Nicolet spectrophotometer in the range 4000–400 cm^{-1}. Electronic spectra were obtained on a diode array Agilent 8453 spectrophotometer in the spectral window 190–1100 nm at room temperature using methanol solutions at 0.001 mol L^{-1}. Magnetic moment determinations were made in solid-state using a Sherwood Scientific Mark 1 magnetic susceptibility balance. Conductivity measurements were performed using a Jenway pH-

conductimeter model 4330 in 0.001 mol L^{-1} solutions in MeOH. JEOL JES-TE300 spectrometer with X-Band at 100 kHz modulation frequency and a cylindric cavity in the mode TE$_{011}$ was employed to perform EPR spectra, all experiments were carried out employing 0.003 mol L^{-1} methanolic solutions at 77 K.

2.3. Synthesis and physicochemical data

Detailed synthetic methods and experimental physicochemical data can be consulted in the ESI.†
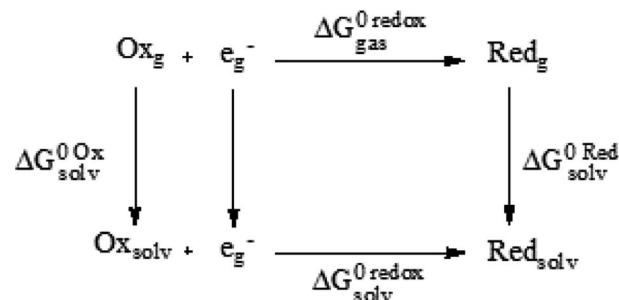
2.4. Electrochemical measurements

Cyclic voltammetry experiments were carried out with 0.001 mol L^{-1} solutions of the corresponding compound in DMSO. Employed solutions contained 0.1 mol L^{-1} of tetra-N-butylammonium hexafluorphosphate (TBAPF$_6$). A potentiostat/galvanostat BioLogic SP-300 was used to record the experiments. A typical three-electrode array cell was implemented: glassy carbon disk ($\phi = 2$ mm) as the working electrode, a platinum wire served as a counter-electrode, and a silver wire as a pseudo-reference electrode. Before each measurement, the solutions were bubbled with nitrogen and the working electrode was rinsed with distilled water to be placed into an ultrasonic bath. Voltammograms were initiated from open circuit potential (E_{ocp}) and scan rates of 10, 50, 100, 250, 500, 750, and 1000 mV s^{-1} were employed in both oxidative and reductive directions. Potentials were reported *versus* the couple Fc/Fc$^+$ ($\Delta E_P = 65$ mV, $\nu = 0.1$ V s^{-1}) according to IUPAC convention.[66] Voltammograms are obtained at $\nu = 0.2$ V s^{-1}.

2.5. Computational details

DFT calculations were performed with Gaussian 09 package,[67] using M06 functional[68] in conjunction Los Alamos LanL2DZ.[69–71] This methodology has been already used to study metal-containing systems.[72–76] All structures were confirmed as minima on the potential energy surface through the vibrational frequency analysis (0 imaginary frequencies). Molar volume was obtained with a single-point calculation based on optimized structures and Molecular Electrostatic Potential (MEP) was plotted as a guide to assess charge distribution and global reactivity.

To calculate redox potentials, we followed previous reports that have proven to be useful for transition metal complexes,[77–79] and in which geometries of ferrocene (Cp$_2$Fe) and ferrocenium ([Cp$_2$Fe]$^+$) in the eclipsed conformation (D_{5h}) were taken into account and optimized in the gas phase. Gas phase and solvation ΔG energies were calculated by the same level of theory and using SMD continuum solvation model[80] and DMSO to simulate the same environment of the electrochemical experiments. To obtain gas phase and solvation free energies of all species, a thermochemical analysis at 298.15 K and 1 atm were performed following the next cycle:

Redox potential was determined through the free energy changes and according to the one-electron exchange of Nernst equation:

$$\Delta G_{solv}^{0\ redox} = \Delta G_{gas}^{0\ redox} + \Delta G_s^{0\ red} - \Delta G_s^{0\ ox} \qquad (1)$$

$$\Delta G_{solv}^{0\ redox} = -F E_{calc}^0 \qquad (2)$$

where F is the Faraday constant. The values are doubly referenced first, to the standard hydrogen electrode, which in MeCN has a value of 4.6 V (ref. 81) and second to a value of 0.68 V for Cp$_2$Fe estimated by the same level of theory to agree with the experimental measurements.

2.6. Antiproliferative activity

The antiproliferative activity was performed on a cell line of epithelial human cervix cancer (HeLa) and was determined by the 3-(4,5-dimethylthiazol-2-yl)-2,5-diphenyltetrazolium bromide (MTT) assay[82] by three independent assays performed by triplicate. For each experiment 1×10^4 cells were added to each 96-well plate with DMEM 5% FBS medium and a range from 0.05 to 100 μg mL^{-1} of copper coordination compound previously dissolved in DMSO 2% (v/v). The cultures were incubated for 24 h at 37 °C and 5% CO$_2$ atmosphere. In the last four hours of incubation, cells were washed with a PBS buffer and then 100 μL of DMEM 5% FBS medium and 10 μL of MTT (5 mf + g/m) were added. The absorbance of final solutions was measured in an ELISA iMark Microplate Absorbance Bio-Rad using 630 nm as the reference wavelength. The proliferation rate was determined by linear regression using GraphPad Prism 5.[83] To determine IC$_{50}$, a one-way analysis of variance and Tukey's rang test were analyzed using Sigma Stat® software. Results are shown as an average of the triplicate tests and significant differences are considered when $p < 0.05$.

2.7. Synthesis of CS–NIPAAm hydrogel

The hydrogel was synthesized dissolving 1 mmol of CS in 500 mL of water with 5 mL of acetic acid, the solution was purged by bubbling a nitrogen flow through. Then, 1 mmol of N-isopropylacrylamide (NIPAAm) and 0.21 g of N,N'-methylenebis(acrylamide) (MBA) previously dissolved and purged were added. While stirring, the solution was heated up to 70 °C and subsequently, 1% mol of tetramethylethylenediamine (TEMED) and 0.7 g of ammonium persulfate (APS) were added to catalyze and start polymerization, respectively. The reaction occurred during the next 24 h. The solution was centrifugated to 2598 rcf

and the supernatant was lyophilized at $-35\ °C$ and 0.035 mbar for 24 h under N_2 atmosphere.

2.8. Characterization of CS–NIPAAm hydrogel

FT-IR spectra were recorded on KBr disks in a Nexus Thermo Nicolet spectrophotometer in the range 4000–400 cm^{-1}. The hydrodynamic diameter was measured in a HOAc/NaOAc (pH = 5.0) and an H_2NaPO_4/HNa_2PO_4 (pH = 7.4) buffers solutions at 25 and 37 $°C$ using a Zetasizer Nano Zen 3600. Results were analyzed employing Malvern Zetasizer 7.12 software. Differential scanning calorimeter DSC was measured in a DSC1 Mettler Toledo in a cycling regime from 25 to 60 $°C$, from 60 to 25 $°C$ and from 25 to 60 $°C$ with 2 $°C$ per minute as increment. Scanning electron microscopy was performed using a device JEOL 7600, the samples were prepared with a droplet of the hydrogel dispersion in 1 mL buffers solutions of HOAc/NaOAc (pH = 5.0) or H_2NaPO_4/HNa_2PO_4 (pH = 7.4) according to the case, subsequently, a drop of the dispersion (pH = 5.0 or pH = 7.4) was placed over a carbon tape and, after solvent evaporation, samples were covered with gold using sputtering.

2.9. Encapsulation and *in vitro* drug release

All quantifications of [Cu(4,7-dimethyl-1,10-phenanthroline)(*Indo*)]NO_3 were obtained by UV at 271 nm. The encapsulation was accomplished by mixing 2 mL of a hydrogel dispersion (0.01 mg L^{-1} in a buffer HOAc/NaOAc at pH = 5.0) with 1 mL of [Cu(4,7-dimethyl-1,10-phenanthroline)(*Indo*)]NO_3 solution (0.006 mol L^{-1} or 4.275 mg L^{-1} in MeOH), the mixture remained stirring during 36 h, six independent assays were performed. The release was studied at 37 $°C$ employing HOAc/NaOAc (pH = 5.0) buffer and H_2NaPO_4/HNa_2PO_4 (pH = 7.4) buffer, three independent assays were performed for each pH. Samples were collected at different times (0.5, 1, 1.5, 2, 2.5, 3, 6, 9, 24, 27, 31 and 55 h) until not changes were observed. The release behavior was analyzed using the DDSolver complement of Microsoft Excel-2007, and zero-order, first-order, Higuchi, Korsmeyer–Peppas, and Peppas–Sahlin models. The goodness of fit was determined for the highest correlation coefficient (RSQR) and the sum of squares (MSC), and the lowest standard deviation (SS) and Akaike criterion (AIC).

3. Results and discussion

3.1. Synthesis and characterization

Scheme 1 presents the two general synthetic routes followed to obtain the complexes under study. $Cu(NO_3)_2\cdot2.5H_2O$ and HIndo (the free form of indomethacin) are common precursors of the synthesis, and the only difference resides in the diimine employed (pristine and methyl substituted 1,10-phenanthrolines and 2,2′-bipyridines). The general formula of these complexes is [Cu(N–N)(*Indo*)]NO_3, in which *Indo* is the deprotonated form of indomethacin and N–N are different methyl substituted bipyridines and phenanthrolines. The global charge of these systems is positively charged (+1). To study these complexes, two main compound groups were established. The first includes all the 1,10-phenanthrolines molecules and the second contains all the 2,2′-bipyridines derivatives.
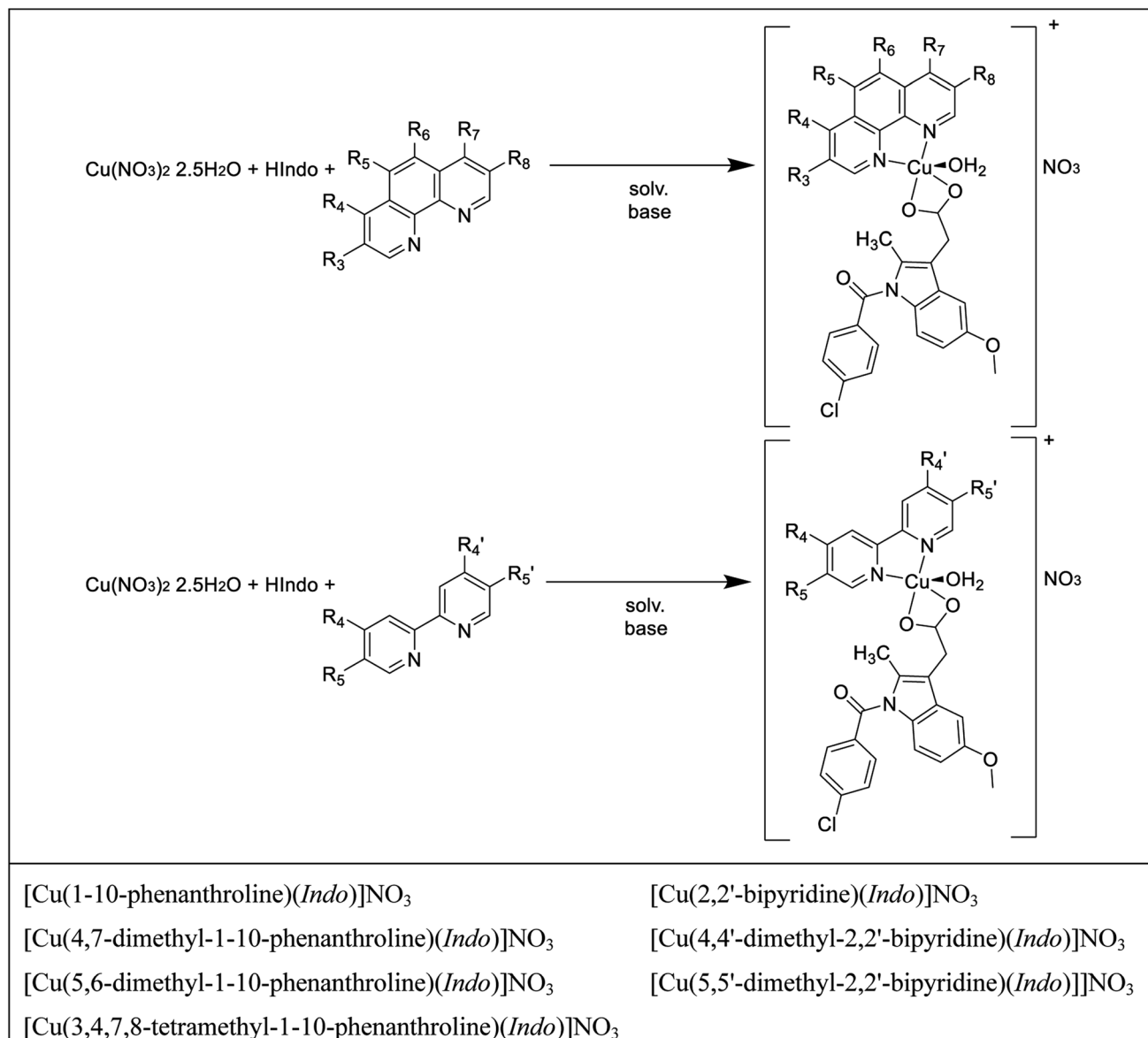
3.2. Spectroscopic and electrochemical characterization

The complete characterization data for the new compounds can be founded in the S1 section of the ESI.† IR spectra (Fig. S1†) analysis indicates the adsorption HIndo band at 3372 cm^{-1}, corresponding to $\nu(OH)$ stretching vibration of carboxylic acid. The disappearance of this band, besides the shift from 1690 cm^{-1} to 1620 cm^{-1} corresponding to the $\nu(C=O)$ stretching vibration suggests that *Indo* is properly coordinated to the Cu atom by the carboxylate groups. Additionally, all compounds' spectra show an absorption band around 3400 cm^{-1}, corresponding to the $\nu(OH)$ vibration, probably caused by the presence of coordinated water on axial positions, and 1385 cm^{-1} associated with the NO_3^- as counterion.[84] Mass spectra (Fig. S2†) of the complexes show the molecular ion [M$^+$] peaks in the range of 577–741 m/z ratio and they are in accordance with the proposed molecular formulae. In addition, conductivity evaluations in a range from 82.4 to 105.9 ohm^{-1} $cm^2\ mol^{-1}$ indicate 1 : 1 electrolyte behavior, in agreement with FTIR. Moreover, μ_{eff} values range from 1.66 to 2.22 BM, which is expected for mononuclear Cu(II) compounds with d^9 configuration ($S = 1/2$), allowing EPR characterization.[85]

The EPR spectra (Table S1 and Fig. S3†) showed $g_{//} < 2.3$, which indicates Cu–L bonds have dominant covalent character, this is explained by the σ-donor capacity of diimines and the electronic inductive effect caused by methyl groups.[86] According to Peishach and Blumberg, $A_{//}$ and $g_{//}$ are useful to determinate the nature of the atoms bonded to copper, the data behavior shows copper centers have mixed copper–nitrogen and copper–oxygen bonds (CuN_2O_2 center).[87] Dependence $g_{//} > g_\perp > g_e$ purpose that the unpaired electron is in the $d_{x^2-y^2}$ orbital, suggesting copper centers with axial symmetry D_{4h} (square planar or octahedral with distortion) and confirming mixed copper–nitrogen and copper–oxygen bonds. Consistent with A_{iso} and g_{iso} values, the geometry adopted by all compounds is square-based pyramid C_{4v}.[86,88] The small f values ($f = g_{//}/A_{//}$) showed by the seven copper compounds demonstrate their low distortion.[89]

Furthermore, for the systems under examination, λ_{max} transitions (at 230 and 290 nm and $\varepsilon \approx$ 10 000 $M^{-1}\ cm^{-1}$) correspond to transitions from π bonding orbitals to π antibonding orbitals of diimine aromatic rings. The metal–ligand charge transfer from d orbitals with $t_{2g}^6 e_g^3$ configuration to empties π antibonding orbitals are found around 310 nm ($\varepsilon \approx$ 5000 $M^{-1}\ cm^{-1}$).[85,90] Finally, $^2B_1 \rightarrow {}^2E$ and $^2B_1 \rightarrow {}^2B_2$ transitions are observed at 650 nm ($\varepsilon \approx$ 35 $M^{-1}\ cm^{-1}$) and 765 nm ($\varepsilon \approx$ 20 $M^{-1}\ cm^{-1}$), respectively.[91,92]

Solution stability of the compounds was studied at different conditions time: 0–55 h, $T = 22–40\ °C$ and pH = 3.4–8.4 (37 $°C$) by UV-Vis techniques. As an example, the spectra of [Cu(4,7-dimethyl-1,10-phenanthroline)(*Indo*)]NO_3 are presented in Fig. S4–S6.† Regarding this, the metal complexes were stable at the conditions tested, neither the dissociation of the ligands nor the formation of unknown species was detected.

Cu(NO₃)₂ 2.5H₂O + HIndo +

[Cu(1-10-phenanthroline)(*Indo*)]NO₃

[Cu(4,7-dimethyl-1-10-phenanthroline)(*Indo*)]NO₃

[Cu(5,6-dimethyl-1-10-phenanthroline)(*Indo*)]NO₃

[Cu(3,4,7,8-tetramethyl-1-10-phenanthroline)(*Indo*)]NO₃

[Cu(2,2'-bipyridine)(*Indo*)]NO₃

[Cu(4,4'-dimethyl-2,2'-bipyridine)(*Indo*)]NO₃

[Cu(5,5'-dimethyl-2,2'-bipyridine)(*Indo*)]]NO₃

Scheme 1 The seven heteroleptic complexes of Cu^{II} under study.

Cyclic voltammetry was carried out to use half-wave potentials values ($E_{1/2}$ for the Cu^{II}/Cu^{I} process) as possible descriptors related to the biological activity. Fig. 1 shows the voltammogram of [Cu(4,4′-dimethyl-2,2′-bipyridine)(*Indo*)]NO₃ acquired with a glassy carbon electrode from open circuit potential to cathodic direction. Neither 1,10-phenanthroline and 2,2′-bipyridine nor HIndo processes interfere with copper signals.[93] A peak was assigned to the copper reduction process at approximately −0.78 V/Fc^{+}–Fc, and its respective oxidative (Cu^{I} → Cu^{II}) process was detected around at −0.55 V/Fc^{+}–Fc. Even though some other signals can be found in the systems analyzed, for this study, only Cu^{II}/Cu^{I} redox values were considered. In general, the systems under study present a quasi-reversible behavior and since cathodic peak currents are not proportional to $v^{1/2}$, non-diffusion-controlled processes are

implied. Half-wave potentials are presented in Table 1 for all the investigated complexes.

Table 1 presents the redox potential values for copper(ɪɪ) mixed compounds. It has been already suggested that this redox potential could play a key role in modulating the biological activity for some metal-containing systems, including copper.[29] For the complexes under study, $E_{1/2}$ for Cu^{I}/Cu^{II} redox pair are in a range between −0.63 and −0.83 V/Fc^{+}–Fc values. In general, higher redox potential values are found in complexes containing 1,10-phenanthroline ligands. This can be explained by the extra aromatic ring compared to the 2,2′-bipyridine systems. The enhancement of the aromaticity is related to the electron delocalization capability. In those systems, this feature can explain the electron density decreasing around the copper atom through π back-bonding, thus, facilitating its reduction. Besides, methyl substituted systems can produce an electron
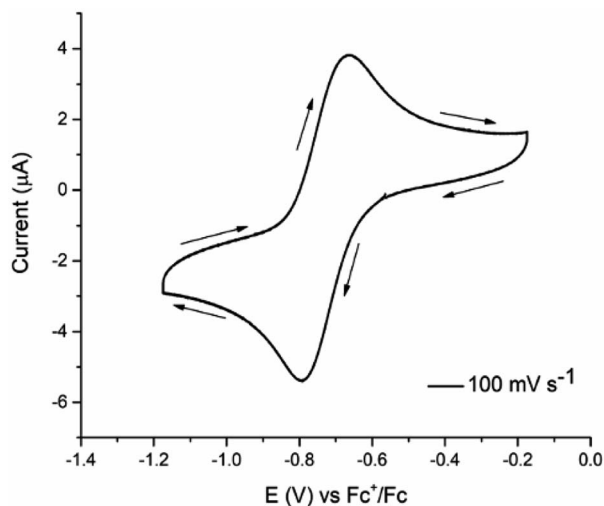
Fig. 1 Cyclic voltammogram of 0.001 mol L^{-1} [Cu(4,4′-dimethyl-2,2′-bipyridine)(*Indo*)]NO$_3$, 0.1 mol L^{-1} TBAPF$_6$ in DMSO, v = 0.1 V s^{-1}.

density increased nearby the metal center by σ donation, without reducing the π back-bonding diimines capabilities as observed for [Cu(3,4,7,8-tetramethyl-1,10-phenanthroline)(*Indo*)]NO$_3$.

3.3. Antiproliferative activity

The half inhibitory concentration (IC$_{50}$, μmol L^{-1}) results for the *in vitro* evaluation on HeLa cervical cancer cells for the new third Casiopeinas® generation with indomethacin is presented in Table 2. Cisplatin is one of the most common drugs for treating cancer and its IC$_{50}$ is also presented for comparison purposes (IC$_{50}$ = 12.5 μmol L^{-1} and Log IC$_{50}$ = 1.10). Also, IC$_{50}$ for Cu(NO$_3$)$_2$ is shown to truly assess the importance of copper complexes compared to Cu(II) in an aqueous solution (IC$_{50}$ > 100.00 μmol L^{-1}). The obtained values present a short-range since few structural modifications are present, *i.e.* the only differences are the number of aromatic rings and the presence in some compounds of methyl groups in different positions. This is related to the electron delocalization efficiency and the electron donating and withdrawing capability of each system. In this regard, IC$_{50}$ values vary from 0.67 to 25.20 μmol L^{-1}. According to the established compounds groups, substituted 1,10-phenanthroline systems showed higher antiproliferative activity compared to substituted 2,2′-bipyridine compounds. In

each complex group, the less active system corresponds to those that are not substituted, *i.e.* [Cu(1,10-phenanthroline)(*Indo*)] NO$_3$ and [Cu(2,2′-bipyridine)(*Indo*)]NO$_3$ with IC$_{50}$ values of 2.3 and 25.2 μmol L^{-1}, respectively. This trend is in good agreement with previous Casiopeinas® reports[29] and excluding [Cu(2,2′-bipyridine)(*Indo*)]NO$_3$, all the analyzed systems show a lower IC$_{50}$ value compared to cisplatin. In this regard, indomethacin derivatives show higher antiproliferative efficiency than the acetylacetonate derivatives.[29] The trend in the primary donor is the same in both class of compounds, thus indicating that the difference arises from the secondary ligand. The inherent antiproliferative properties of the indomethacin can enhance the cytotoxic behavior of the copper compound.

From all the studied complexes, [Cu(5,6-dimethyl-1,10-phenanthroline)(*Indo*)]NO$_3$ and [Cu(4,7-dimethyl-1,10-phenanthroline)(*Indo*)]NO$_3$ are the most effective (IC$_{50}$ = 0.67 and 0.72 μmol L^{-1}, respectively). Those systems are characterized by having three aromatic rings and –CH$_3$ groups in different positions, which enables them to promote a better electron delocalization and to increment electron density on the copper metal atom. Usually, copper containing compounds might offer some advantages. They have high stability in physiological conditions, could be safer in comparison to other metal complexes, and they can produce several cell death mechanisms including cuproptosis or apoptosis.[27,34] Hence, six of seven synthesized compounds belonging to the third Casiopeinas® generation with indomethacin might be suitable and considered as promising candidates for further studies as metallodrugs against cancer. Furthermore, those trends are in concordance with previous inquiries[29,33,34] in which copper complexes are assumed to react with some important endogen reducers molecules such as glutathione and nicotinamide adenine dinucleotide (NADH). These reactions can generate Cu(I) species, which in turn can react with molecular oxygen (O$_2$), hydrogen peroxide (H$_2$O$_2$), and superoxide radical (O$_2^{·-}$) producing reactive oxygen species, thus causing oxidative damage and mitochondrial dysfunction.[34] Finally, for the subsequent analysis, we have selected as the drug model for hydrogel design, [Cu(4,7-dimethyl-1,10-phenanthroline)(*Indo*)] NO$_3$ compound.

3.4. Physicochemical indexes related to the antiproliferative activity

To simulate the molecular geometry and recognize the physicochemical features that describe the antiproliferative activity,

Table 1 Redox potential ($E_{1/2}$)

Compounds	$E_{1/2}$ Cu^I/Cu^{II} (V/Fc$^+$–Fc)
[Cu(1,10-phenanthroline)(*Indo*)]NO$_3$	−0.66
[Cu(4,7-dimethyl-1,10-phenanthroline)(*Indo*)]NO$_3$	−0.83
[Cu(5,6-dimethyl-1,10-phenanthroline)(*Indo*)]NO$_3$	−0.63
[Cu(3,4,7,8-tetramethyl-1,10-phenanthroline)(*Indo*)]NO$_3$	−0.65
[Cu(2,2′-bipyridine)(*Indo*)]NO$_3$	−0.65
[Cu(4,4′-dimethyl-2,2′-bipyridine)(*Indo*)]NO$_3$	−0.72
[Cu(5,5′-dimethyl-2,2′-bipyridine)(*Indo*)]NO$_3$	−0.76

Table 2 IC$_{50}$ results against HeLa cervical cancer cells

Compounds	IC$_{50}$ (μmol L^{-1})	Log (IC$_{50}$)	IC$_{50}$ acac^a (μmol L^{-1})
Cisplatin	12.5 ± 0.70	1.10	—
[Cu(1,10-phenanthroline)(*Indo*)]NO$_3$	2.30 ± 0.02	0.36	10.7 ± 0.9
[Cu(4,7-dimethyl-1,10-phenanthroline)(*Indo*)]NO$_3$	0.72 ± 0.10	−0.14	1.4 ± 0.1
[Cu(5,6-dimethyl-1,10-phenanthroline)(*Indo*)]NO$_3$	0.67 ± 0.02	−0.17	3.4 ± 0.5
[Cu(3,4,7,8-tetramethyl-1,10-phenanthroline)(*Indo*)]NO$_3$	1.00 ± 0.03	0.00	1.9 ± 0.2
[Cu(2,2′-bipyridine)(*Indo*)]NO$_3$	25.2 ± 1.07	1.40	42.0 ± 3.1
[Cu(4,4′-dimethyl-2,2′-bipyridine)(*Indo*)]NO$_3$	7.87 ± 0.40	0.90	18.2 ± 2.7
[Cu(5,5′-dimethyl-2,2′-bipyridine)(*Indo*)]NO$_3$	2.87 ± 1.02	0.46	N.R.
Cu(NO$_3$)$_2$	>100	>2	—

^{a} Ref. 29, N.R.: not reported.

DFT optimizations, molar volume (V), and redox potential E^0_{calc} calculations were performed. Fig. S7† shows the optimized geometries and the calculated values of V and E^0_{calc}.

The Cu^{II} complexes present a square planar arrangement where the indomethacin and diimines are both bidentate O–O (C–O distance average 1.97 Å) and N–N (Cu–N distance average 1.97 Å) coordinated, respectively. The reduced Cu^I species has a trigonal planar geometry, the diimine remains N–N bonded (Cu–N distance average 1.92 and 1.99 Å) and the indomethacin is bonded only for a single O atom (Cu–O average distance 1.90 Å). The remaining oxygen atom remains far from the Cu atom, but still, a weak intermolecular interaction could be proceeding (Cu–O average distance 3.02 Å).

By QSAR studies, our research group demonstrates that the cytotoxic activity of the first Casiopeinas® generation can be described by the redox potential.[29,94,95] The redox potential has been used commonly in structure–activity studies for several metal containing compounds with biological activity.[94] Although calculated redox potential values, E^0_{calc}, are in good agreement with experimental ones ($R^2 = 0.98$, Fig. S8†), in this case; this parameter does not provide useful information regarding the antiproliferative effect. However, when the molar volume, V, is employed, some interesting relations can be made. In Fig. 2, we present those correlations for the two involved

compound families. On the one hand, the 1,10-phenanthroline group, and on the other hand the 2,2′-bipyridine molecules. As can be seen in this Fig. 2, only the molar volume was considered, and molecules are well separated according to the group they belong to (black circles for 2,2′-bipyridine molecules and red squares for 1,10-phenanthroline compounds, with $R^2 = 0.9998$, and $R^2 = 0.9117$, respectively). The most important result from this figure, is that for all complexes under study, the larger the volume, the better the antiproliferative effect. This trend can be observed regardless of the molecules group. In particular, the steric effect is much more pronounced on the cytotoxic efficiency for bipyridine derivatives compared to phenanthroline ones. As previously observed, the less active complexes correspond to the non-methylated substituted complexes. Contrarily, comparing methyl substitutions, the one in position 5 enhances the biological activity. Interestingly, the 5,6-dimethyl-1,10-phenanthroline derivative shows the best cytotoxic behavior. This complex owns the most oxidizing power and the biggest molar volume of all the analyzed systems. In this regard, it has been proved that this ligand enhances the capability of Casiopeinas® of diffusion across the cell membrane due to the minimized electronic and structural repulsion provided by the methyl substitution in the 5,6-positions compared to others.[93] Accordingly, the change in the
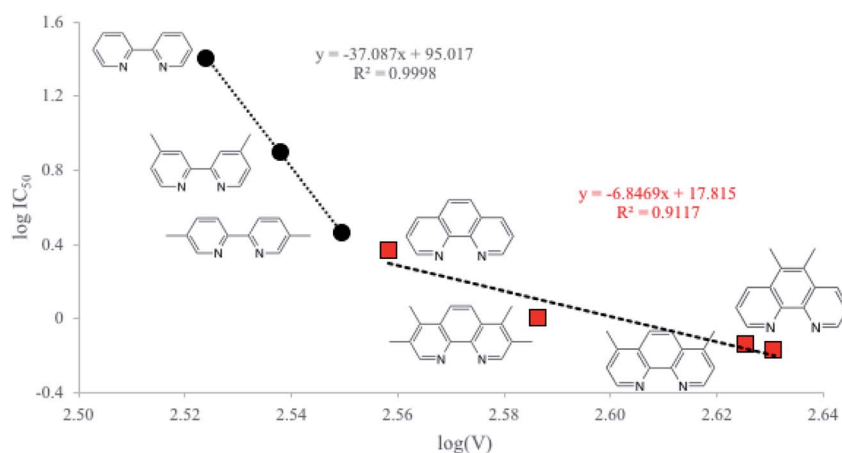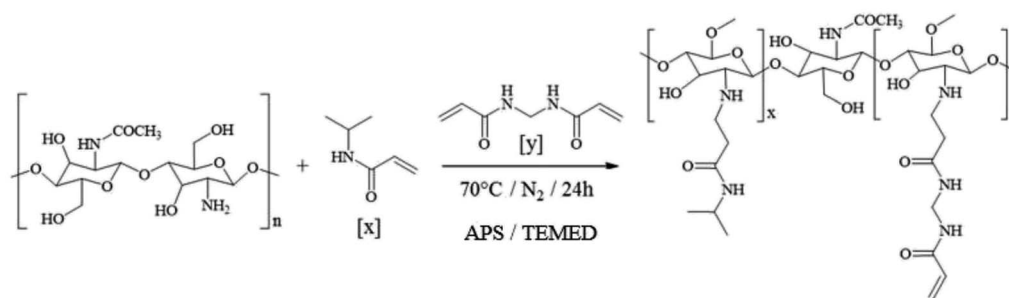

Fig. 2 Antiproliferative activity and molar volume relations.

APS=Ammonium persulfate, TEMED: Tetramethylendiamine

Scheme 2 Scheme of CS–NIPAAm synthesis.

biological activity can be attributed to the interactions that facilitate their passage through the membrane, that is, its biodistribution.

3.5. Synthesis and physicochemical characterization of chitosan–PNIPAAm nanogel

The CS–PNIPAAm nanogel was obtained as a slightly cloudy dispersion with a pH value of 6.0. The polymerization reaction is carried out by free radical generation. For this kind of synthesis is extremely important to keep the reaction mixture in oxygen-free conditions and protected from visible light to conserve the polymerization control.[96] Scheme 2 shows the synthetic path.

The characterization of the nanogel was made by FT-IR spectroscopy. The signals in 1648 (ν_s C=O), 1553 (ν_{as} N–H), and 1261 cm^{-1} (ν_s C–N) confirm the presence of the amide group.[97] Broadband around 1066 cm^{-1} is according to the

pyranosic ring.[98] Additionally, the bending of methylene of the methylene group (ν_{sc} C–H) that produces a signal in 1469 cm^{-1} can be observed.[98] Finally, the peak in 1027 cm^{-1} is attributed to the ether groups (ν_s C–O–C).[98]

To emulate biological conditions and to evaluate the behavior of the nanogel in those situations, various characterization parameters were obtained at different temperatures and pH values. Table 3 contains the obtained hydrodynamic diameter, zeta potential (Z_p), and polydispersity index (PDI).

PDI values indicate that, in the studied conditions, the nanogel is not a monodisperse system. The temperature does not have a great effect on the hydrodynamic diameter, nevertheless, the particles swell when pH values diminish; these results are explained by the polymers ratio minish in the hydrogel. The swelling in acidic conditions can be explained since at low pH values, the lateral chains of CS are protonated, and thus, repulsion is increased and so is the hydrodynamic diameter. In the same way, the acidic pH generates a positive potential difference while the neutral polymer (pH = 7.4) has a negative Z_p value. Anyway, in both values of investigated pH, the CS–NIPAAm polymer is electrically stable. The difference in the revised indexes suggests that the polymer responds to pH and temperature changes.[99]

The changes in the differential calorimetry screening (DSC) study were measured in the range of 25–60 °C. The DSC plot can be founded in Fig. S9.† The free PNIPAAm single transition is observed at 28.07 °C, close to the reported values in the

Table 3 Nanogel characterization indexes

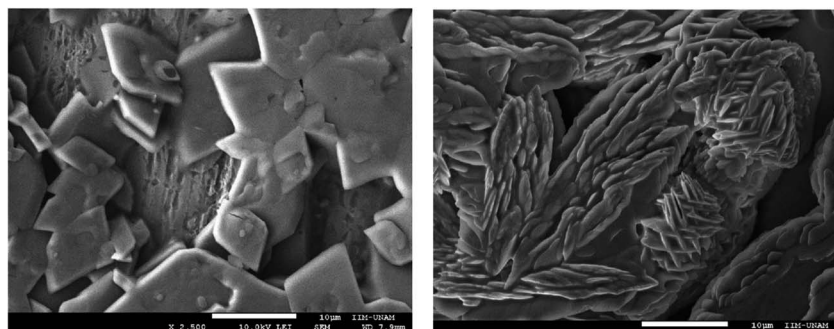| pH	T (°C)	Hydrodynamic diameter (nm)	Z_p (mV)	PDI
5.0	25	690.27 ± 7.10	22.97 ± 0.55	0.530
	37	654.13 ± 32.07	23.50 ± 0.35	0.512
7.4	25	108.92 ± 12.85	−6.81 ± 0.45	0.573
	37	100.89 ± 8.33	−5.81 ± 1.90	0.540

Fig. 3 Micrographs for the nanogel at pH: 5.0 (left) and 7.4 (right).

specialized literature.[100] For the nanogel at pH = 5.0, two transitions are founded, the first at 28.19 °C, that can be attributed to the free NIPAAm, and the second is found at 45.16 °C and can be related to the CS–NIPAAm interaction. At pH = 7.4, a single transition at 49.76 °C was observed. For both examined pH values, the second cycle presents a similar behavior to the first one. The involved energy in the phase transition for pH = 7.4 is -1.20 W g^{-1} and for pH = 5.0 is -0.13 W g^{-1}. Those results in addition to the observed increased temperature for the transition indicate that a stronger interaction between CS and NIPAAm at the higher pH value occurs.[101]

Furthermore, the scanning electron microscopy (SEM) technique was performed and the micrographs are presented in Fig. 3.

The micrographs reveal different morphologies for the different pH conditions. In the acidic situation, the nanogel presents rhombohedral structures with well-defined edges, its size varies between 3–5 μm. At neutral pH, laminar form is observed, the sheets are about 0.11 μm in thickness. While the size at pH = 7.4 correlates well with those reported in Table 3, those at pH = 5.0 are different. This could be explained because of morphology changes by the solvent evaporation. This reveals again, the nanogel pH dependence behavior. Finally, these results suggest that the synthesized nanogel can be used as a drug carrier with a pH dependence.

3.6. Drug encapsulation and release

Antiproliferative assays showed that substituted phenanthroline derivatives present higher cytotoxic efficiency. *In vivo*, previous reports have informed that the 4,7-dimethyl-1,10-phenanthroline analogs shows lower toxicity against healthy cells.[102] For the above, the compound [Cu(4,7-dimethyl-1,10-phenanthroline)(*Indo*)]NO$_3$ was elected to analyze its nanogel encapsulation and release.

The encapsulation was performed in a HOAc/NaOAc buffer solution at pH = 5.0 and 20 °C, which are conditions where the hydrogel is swelled. The encapsulation efficiency (% EE) was defined as the ratio of the weight of [Cu(4,7-dimethyl-1,10-phenanthroline)(*Indo*)]NO$_3$ contained into the hydrogel to the weight of [Cu(4,7-dimethyl-1,10-phenanthroline) (*Indo*)]NO$_3$ added, loading capacity (% LC) was defined as the ratio of the weight of [Cu(4,7-dimethyl-1,10-phenanthroline)(*Indo*)]NO$_3$ contained in the hydrogel to the weight of the hydrogel. Under the studied conditions, the hydrogel reached a % EE = 69.47 ± 1.41 and a % LC = 0.0496 ± 0.0010 (0.9899 ± 0.0201 mg of copper compound for each 20 mg of nanogel). The results are presented in Table S2.†

Fig. 4 shows the percentage of cumulative compound released as a function of time in both pH conditions. It can be observed that drug release depends on the pH value. In acidic conditions, the drug liberation is faster than for the pH = 7.4. In both cases, a Burst effect is observed in the first 6 hours. This effect is produced by the rapid release of the compound that interacts with the nanogel surface compared to that which is embodied in the polymeric membrane.
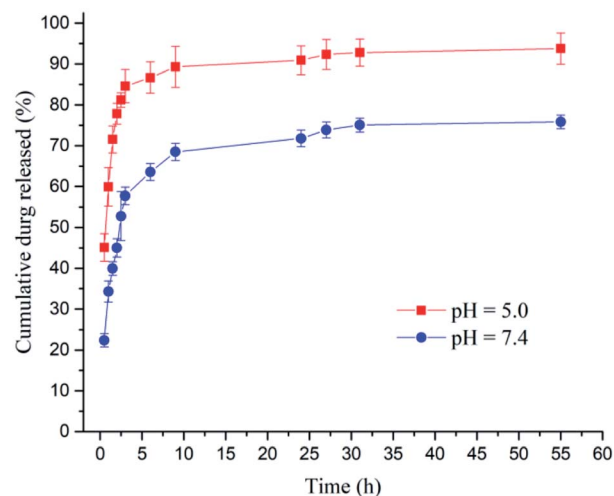

Fig. 4 Percentage of *in vitro* cumulative [Cu(4,7-dimethyl-1,10-phenanthroline)(*Indo*)]NO$_3$ released as a time function.

Table 4 Kinetic parameters of the Peppas–Sahlin model for drug release

Parameter	pH = 5.0	pH = 7.4
k_1	82.402 ± 0.942	40.907 ± 1.815
k_2	−18.350 ± 0.382	−6.397 ± 0.408
m	0.522 ± 0.010	0.665 ± 0.024

To understand the drug release mechanism, some kinetic drug release models were proved to establish the nanogel behavior. For both evaluated pH conditions, the Peppas–Sahlin model provided the best fit (Table 4 and Fig. S10†).[103]

The magnitudes of k_1 compared to k_2 indicates that Fick diffusion controls the drug transport mechanism and the negative values of k_2 suggest an almost inexistent contribution due to polymeric chains relaxation. Also, the m value shows a spherical material. The observations found here agree with the reports from other nanogels and soluble-water compounds.[104] The increased release of this system in the acidic media allows us to propose it as a specific potential drug nanocarrier for the tumoral microenvironment.

4. Conclusions

Seven new copper complexes known as Casiopeinas® were synthesized and characterized by different analytical techniques. Spectroscopic characterization and magnetic measurements of the complexes are in accordance with a square-based pyramid geometry around the metal center. Redox potentials and molar volume are modulated by the nature of the diamine moiety and the methyl substituents positions. In the light of these, also the biological activity can be modulated by the primary donor. The methyl substituents that produce steric effect, can also enhance/decrease the biological activity by their difficult or hinder the passing across the cell membrane, as it

has been established for other members of Casiopeinas®. On the other hand, the cytotoxicity obtained by IC_{50} of the third-generation analogs are higher than the acetylacetonate derivatives first generation compounds, due to the introduction of an active secondary ligand. In general, the most oxidant and bigger complexes show major cytotoxic effect. No quantitative relation between the IC_{50} value and $E_{1/2}$ was founded. Instead, computational calculations, indicate that the molar volume can be used as a descriptor index related to the antiproliferative activity. New CS–PNIPAAm nanogel was synthesized by the copolymerization method. IR and DSC analyses show that the polymer is composed of both started materials and the interaction are more prominent in neutral than acidic environments. Also, in acid conditions, the nanogel suffers swelling due to the protonation of lateral chains. Zeta potential, hydrodynamic diameter, and morphology results suggest that nanogel presents structural changes when the pH is modified. Encapsulation of [Cu(4,7-dimethyl-1,10-phenanthroline)(*Indo*)] NO_3 into the nanogel was performed. The efficiency of this process is close to 70%. The release of the compound presents a Burst effect and it is faster in acid conditions. The release mechanism follows the Peppas–Sahlin model, *i.e.*, it presents a concomitant mechanism of passive diffusion and polymeric chain relaxation.

Funding

Conflicts of interest

The authors declare no conflict of interest.

Acknowledgements

References

1 V. Hodgkinson and M. J. Petris, *J. Biol. Chem.*, 2012, **287**(17), 13549–13555.

2 Z. Huaizhi and N. Yuantao, *Gold Bull.*, 2001, **34**(1), 24–29.

3 K. Strebhardt and A. Ullrich, *Nat. Rev. Cancer*, 2008, **8**(6), 473–480.

4 H. Maruta, *Drug Discoveries Ther.*, 2009, **3**(2), 37–40.

5 B. Rosenberg, L. Vancamp, J. E. Trosko and V. H. Mansour, *Nature*, 1969, **222**(5191), 385–386.

6 D. Lebwohl and R. Canetta, *Eur. J. Cancer*, 1998, **34**(10), 1522–1534.

7 L. Kelland, *Nat. Rev. Cancer*, 2007, **7**(8), 573–584.

8 T. C. Johnstone, K. Suntharalingam and S. J. Lippard, *Chem. Rev.*, 2016, **116**(5), 3436–3486.

9 Institute, N. C. National Cancer Institute, available at: https://www.cancer.gov.

10 E. R. Jamieson and S. J. Lippard, *Chem. Rev.*, 1999, **99**(9), 2467–2498.

11 G. Chu, *J. Biol. Chem.*, 1994, **269**(2), 787–790.

12 V. Cepeda, M. A. Fuertes, J. Castilla, C. Alonso, C. Quevedo and J. M. Pérez, *Anti-Cancer Agents Med. Chem.*, 2007, **7**(1), 3–18.

13 S. Dasari and P. B. Tchounwou, *Eur. J. Pharmacol.*, 2014, **740**, 364–378.

14 A. M. Florea and D. Büsselberg, *Cancers*, 2011, **3**(1), 1351–1371.

15 E. Pérez-Herrero and A. Fernández-Medarde, *Eur. J. Pharm. Biopharm.*, 2015, **93**, 52–79.

16 R. P. Miller, R. K. Tadagavadi, G. Ramesh and W. B. Reeves, *Toxins*, 2010, **2**(11), 2490–2518.

17 M. H. Hanigan and P. Devarajan, *Cancer Ther.*, 2003, **1**, 47.

18 T. T. H. Fong, C. N. Lok, C. Y. S. Chung, Y. M. E. Fung, P. K. Chow, P. K. Wan and C. M. Che, *Angew. Chem., Int. Ed.*, 2016, **55**(39), 11935–11939.

19 A. Hordyjewska, I. Popiołek and J. Kocot, *BioMetals*, 2014, **27**, 611–621.

20 T. Theophanides and J. Anastassopoulou, *Crit. Rev. Oncol. Hematol.*, 2002, **42**(1), 57–64.

21 E. Urso and M. Maffia, *J. Vasc. Res.*, 2015, **52**, 172–196.

22 G. F. Hu, *J. Cell. Biochem.*, 1998, **69**, 326–335.

23 P. E. Tawari, Z. Wang, M. Najlah, C. W. Tsang, V. Kannappan, P. Liu, C. McConville, B. He, A. L. Armesilla and W. Wang, *Toxicol. Res.*, 2015, **4**, 1439–1442.

24 K. Gorshkov, N. Sima, W. Sun, B. Lu, W. Huang, J. Travers, C. Klumpp-Thomas, S. G. Michael, T. Xu and R. Huang, *Transl. Oncol.*, 2019, **12**, 441–452.

25 O. Krasnovskaya, A. Naumov, D. Guk, P. Gorelkin, A. Erofeev, E. Beloglazkina and A. Majouga, *Int. J. Mol. Sci.*, 2020, **21**, 3965.

26 X. Chen, Q. P. Dou, J. Liu and T. Daoling, *Front. Mol. Biosci.*, 2021, **8**, 649151.

27 P. Tsvetkov, A. Detappe, K. Cai, H. R. Keys, Z. Brune, W. Ying, P. Thiru, M. Reidy, G. Kugener, J. Rossen, M. Kocak, N. Kory, A. Tsherniak, S. Santagata, L. Whitesell, I. M. Ghobrial, J. L. Markley, S. Lindquist and T. R. Golub, *Nat. Chem. Biol.*, 2019, **15**(7), 681–689.

28 A. Tovar-Tovar, L. Ruiz-Ramírez, A. Campero, A. Romerosa, R. Moreno-Esparza and M. J. Rosales-Hoz, *J. Inorg. Biochem.*, 2004, **98**(6), 1045–1053.

29 M. E. Bravo-Gómez, J. C. García-Ramos, I. Gracia-Mora and L. Ruiz-Azuara, *J. Inorg. Biochem.*, 2009, **103**(2), 299–309.

30 M. Reina, L. F. Hernández-Ayala, M. E. Bravo-Gómez, V. Gómez and L. Ruiz-Azuara, *Inorg. Chim. Acta*, 2021, **517**, 120201.

31 P. Jiménez Ayala, *Síntesis y Caracterización de 5,6-Dimetil-1,10-Fenantrolina y Derivados Mixtos de Cobre (II)*, School

of Chemistry, Universidad Nacional Autónoma de México, 2015.

32 Y. Figueroa-DePaz, J. Pérez-Villanueva, O. Soria-Arteche, D. Martínez-Otero, V. Gómez-Vidales, L. Ortiz-Frade and L. Ruiz-Azuara, *Molecules*, 2022, **27**(11), 3504.

33 Y. Figueroa-DePaz, K. Resendiz-Acevedo, S. G. Dávila-Manzanilla, J. C. García-Ramos, L. Ortiz-Frade, J. Serment-Guerrero and L. Ruiz-Azuara, *J. Inorg. Biochem.*, 2022, **231**, 111772.

34 R. Kachadourian, H. M. Brechbuhl, L. Ruiz-Azuara, I. Gracia-Mora and B. J. Day, *Toxicol*, 2010, **268**(3), 176–183.

35 J. Serment-Guerrero, P. Cano-Sánchez, E. Reyes-Pérez, F. Velázquez-García, M. E. Bravo-Gómez and L. Ruiz-Azuara, *Toxicol. In Vitro*, 2011, **25**, 1376–1384.

36 J. C. García-Ramos, A. G. Gutiérrez, A. Vázquez-Aguirre, Y. Toledano-Magaña, A. L. Alonso-Sáenz, V. Gómez-Vidales, M. Flores-Álamo and L. Ruiz-Azuara, *BioMetals*, 2017, **30**(1), 43–58.

37 A. De Vizcaya-Ruiz, A. Rivero-Muller, L. Ruiz-Ramirez, G. E. N. Kass, L. R. Kelland, R. M. Orr and M. Dobrota, *Toxicol. In Vitro*, 2000, **14**(1), 1–5.

38 A. Rivero-Müller, A. De Vizcaya-Ruiz, N. Plant, L. Ruiz and M. Dobrota, *Chem.-Biol. Interact.*, 2007, **165**(3), 189–199.

39 C. Campero-Peredo, M. E. Bravo-Gómez, S. L. Hernández-Ojeda, S. del Rosario Olguín-Reyes, J. J. Espinosa-Aguirre and L. Ruiz-Azuara, *Toxicol. In Vitro*, 2016, **33**, 16–22.

40 M. Reina, L. G. Talavera-Contreras, Y. Figueroa-DePaz, L. Ruiz-Azuara and L. F. Hernández-Ayala, *New J. Chem.*, 2022, **46**, 12500–12511.

41 J. R. Vane, *Nat. New Biol.*, 1971, **231**, 232–235.

42 K. M. Leahy, D. L. DeWitt and R. M. Garavito, *Annu. Rev. Biochem.*, 2000, **69**, 145–182.

43 Y. Eli, F. Przedecki, G. Levin, N. Kariv and A. Raz, *Biochem. Pharmacol.*, 2001, **61**(5), 565–571.

44 J. N. Boodram, I. J. McGregor and P. M. Bruno, *Angew. Chem., Int. Ed.*, 2016, **55**, 2845–2850.

45 A. M. Bonin, J. A. Yáñez and C. Fakuda, *Cancer Chemother. Pharmacol.*, 2010, **66**, 755–764.

46 S. Senapati, A. K. Mahanta, S. Kumar and P. Maiti, *Signal Transduction Targeted Ther.*, 2018, **3**(1), 1–19.

47 N. S. Rejinold, M. Muthunarayanan, K. P. Chennazhi, S. V. Nair and R. Jayakumar, *Int. J. Biol. Macromol.*, 2011, **48**(1), 98–105.

48 T. Jain, S. Kumar and P. K. Dutta, *Int. J. Biol. Macromol.*, 2016, **82**, 1011–1017.

49 Y. Li, D. Maciel, J. Rodrigues, X. Shi and H. Tomas, *Chem. Rev.*, 2015, **115**(16), 8564–8608.

50 C. Wischke and A. Lendlein, *Pharm. Res.*, 2010, **27**(4), 527–529.

51 A. Bajpai, S. Shukla, R. Saini and A. Tiwari, *Stimuli Responsive Drug Delivery Systems: From Introduction to Application*, Smithers, 2010.

52 K. Kita and C. Dittrich, *Expert Opin. Drug Delivery*, 2011, **8**(3), 329–342.

53 M. Mahmoudi, H. Hofmann, B. Rothen-Rutishauser and A. Petri-Fink, *Chem. Rev.*, 2012, **112**(4), 2323–2338.

54 C. M. O'driscoll and B. T. Griffin, *Adv. Drug Delivery Rev.*, 2008, **60**(6), 617–624.

55 J. P. Tan, Q. Wang and K. C. Tam, *J. Controlled Release*, 2008, **128**(3), 248–254.

56 A. Astashkina, B. Mann and D. W. Grainger, *Pharmacol. Ther.*, 2012, **134**(1), 82–106.

57 J. K. Oh, R. Drumright, D. J. Siegwart and K. Matyjaszewski, *Prog. Polym. Sci.*, 2008, **33**(4), 448–477.

58 H. K. S. Yadav, N. A. Al Halabi and G. A. Alsalloum, *J. Pharm. Pharmacogn. Res.*, 2017, **1**, 5.

59 L. Zha, B. Banik and F. Alexis, *Soft Matter*, 2011, **7**(3), 5908–5916.

60 Y. Fan, T. Saito and A. Isogai, *Biomacromol*, 2008, **9**(7), 1919–1923.

61 R. A. Muzzarelli, Chitin nanostructures in living organisms, in *Chitin*, Springer, Dordrecht, 2011, pp. 1–34.

62 K. Raemdonck, J. Demeester and S. De Smedt, *Soft Matter*, 2009, **5**(4), 707–715.

63 R. Jayakumar, A. Nair, N. S. Rejinold, S. Maya and N. S. Nair, *Carbohydr. Polym.*, 2012, **87**(3), 2352–2356.

64 Y. W. Chien, *Novel Drug Delivery Systems. Drugs and the Pharmaceutical Sciences*, 1992, p. 50.

65 R. M. Böhmer and G. Morstyn, *Cancer Res.*, 1985, **45**(11), 5328–5334.

66 G. Gritzner and J. Kuta, Recommendations on reporting electrode potentials in nonaqueous solvents (Recommendations 1983), *Pure Appl. Chem.*, 1984, **56**(4), 461–466.

67 M. J. Frisch, G. W. Trucks, H. B. Schlegel, G. E. Scuseria, M. A. Robb, J. R. Cheeseman, G. Scalmani, V. Barone, B. Mennucci and G. A. Petersson, *et al.*, *Gaussian 09*, Gaussian, Inc., Wallingford, CT, USA, 2009.

68 Y. Zhao and D. G. Truhlar, *Theor. Chem. Acc.*, 2008, **120**, 215–241.

69 M. Dolg, U. Wedig, H. Stoll and H. Preuss, *J. Chem. Phys.*, 1987, **86**, 866–872.

70 M. Dolg, U. Wedig, H. Stoll and H. Preuss, *J. Chem. Phys.*, 1989, **90**, 1730–1734.

71 W. R. Wadt and P. J. Hay, *J. Chem. Phys.*, 1985, **82**, 284–298.

72 M. Reina, W. T. Wallace, R. B. Wyrwas, R. L. Whetten and A. Martínez, *Int. J. Quantum Chem.*, 2019, e25987.

73 M. Reina and A. Martínez, *Comput. Theor. Chem.*, 2018, **1130**, 15–23.

74 M. Reina and A. Martínez, *Comput. Theor. Chem.*, 2017, **1120**, 24–33.

75 M. Reina and A. Martínez, *Comput. Theor. Chem.*, 2017, **1112**, 1–9.

76 M. Reina and A. Martínez, *Comput. Theor. Chem.*, 2017, **1099**, 174–184.

77 L. Yan, Y. Lu and X. Lia, *Phys. Chem. Chem. Phys.*, 2016, **18**, 5529–5536.

78 M. M. Flores-Leonar, R. Moreno-Esparza, V. M. Ugalde-Saldívar and C. Amador-Bedolla, *Comput. Theor. Chem.*, 2017, **1099**, 167–173.

79 P. Zerón, J. Carmona-Espíndola, M. M. Flores-Leonar, J. L. Gázquez, I. González, C. Amador-Bedolla and V. M. Ugalde-Saldívar, *ChemistrySelect*, 2018, **3**, 7541–7547.

80 A. V. Marenich, C. J. Cramer and D. G. Truhlar, *J. Phys. Chem. B*, 2009, **113**, 6378–6396.

81 S. Trasatti, *Pure Appl. Chem.*, 1986, **58**(7), 955–966.

82 T. Mosmann, *J. Immunol. Methods*, 1983, **65**(1–2), 55–63.

83 *Linear Regression was Performed Using GraphPad Prism version 5.04 for Windows*, GraphPad Software, La Jolla, California, USA.

84 K. Nakamoto, *Infrared and Raman Spectra of Inorganic and Coordination Compounds*, Wiley Interscience, 2009, DOI: 10.1002/9780470405840.

85 R. S. Drago, *Physical Methods for Chemists*, 1992.

86 D. Kivelson and R. Neiman, *J. Chem. Phys.*, 1961, **35**(1), 149–155.

87 J. Peisach and W. E. Blumberg, *Arch. Biochem. Biophys.*, 1974, **165**(2), 691–708.

88 E. Garribba and G. Micera, *J. Chem. Educ.*, 2006, **83**(8), 1229.

89 M. Łabanowska, E. Bidzińska, A. Para and M. Kurdziel, *Carbohydr. Polym.*, 2012, **87**(4), 2605–2613.

90 J. C. García-Ramos, R. Galindo-Murillo, A. Tovar-Tovar, A. L. Alonso-Saenz, V. Gómez-Vidales, M. Flores-Alamo, L. Ortiz-Frade, F. Cortes-Guzmán, R. Moreno-Esparza, A. Campero and L. Ruiz-Azuara, *Chem.–Eur. J.*, 2014, **20**, 13730–13741.

91 J. E. Huheey, E. A. Keiter, R. L. Keiter and O. K. Medhi, *Inorganic Chemistry: Principles of Structure and Reactivity*, Pearson Education India, 2006.

92 Y. R. Morgan, P. Turner, B. J. Kennedy, T. W. Hambley, P. A. Lay, J. R. Biffin, H. L. Regtop and B. Warwick, *Inorg. Chim. Acta*, 2001, **324**(1–2), 150–161.

93 A. B. P. Lever, Surface electrochemistry of inorganic complexes, *Pure Appl. Chem.*, 1998, **70**(4), 755–763.

94 K. Nesměrák, *Mini-Rev. Med. Chem.*, 2020, **20**(14), 1341–1356.

95 J. C. García-Ramos, G. Vértiz-Serrano, L. Macías-Rosales, R. Galindo-Murillo, Y. Toledano-Magaña, J. P. Bernal, F. Cortes-Guzmán and L. Ruiz-Azuara, *Eur. J. Inorg. Chem.*, 2017, **12**, 1728–1736.

96 V. R. Patel and M. M. Amiji, *pH-Sensitive Swelling and Drug-Release Properties of Chitosan—Poly (Ethylene Oxide) Semi-Interpenetrating Polymer Network*, 1996, pp. 209–220.

97 M. Badertscher, P. Bühlmann and E. Pretsch, *Structure Determination of Organic Compounds*, Springer Berlin Heidelberg, 2009.

98 R. L. Garzón, A. S. Rodrigo, M. N. Montiel, J. N. Pérez, A. B. Garcia and C. V. Calahorro, *Thermochim. Acta*, 1985, **96**(1), 59–68.

99 W. Xiong, W. Wang, Y. Wang, Y. Zhao, H. Chen, H. Xu and X. Yang, *Colloids Surf., B*, 2011, **84**(2), 447–453.

100 O. Czakkel, B. Berke and K. László, *Eur. Polym. J.*, 2019, **116**, 106–116.

101 M. A. Haq, Y. Su and D. Wang, *Mater. Sci. Eng., C*, 2017, **70**, 842–855.

102 J. Serment-Guerrero, P. Cano-Sánchez, E. Reyes-Pérez, F. Velázquez-García, M. E. Bravo-Gómez and L. Ruiz-Azuara, *Toxicol. In Vitro*, 2011, **25**(7), 1376–1384.

103 N. A. Peppas and J. J. Sahlin, *Int. J. Pharm.*, 1989, **57**(2), 169–172.

104 R. B. Baggi and N. B. Kilaru, *Asian Journal of Pharmacy and Technology*, 2016, **6**(4), 223–230.